Original Article
ISSN (Online): 2454-1907

International Journal of Engineering Technologies and Management Research
February 2025 12(2), 1–23

ENERGY ANALYSIS OF A SOLAR-OPERATED SWEEPING GAS MEMBRANE DISTILLATION SYSTEM INTEGRATED WITH DIFFERENT WATER VAPOR CONDENSATION CONFIGURATIONS

Abdullah H. Kadhum [1], Omar A. Bamaga [2], Zulfa A. Baz [3], Nidal H. Abu-Hamdeh [1]

[1] Department of Mechanical Engineering, Faculty of Engineering, King Abdulaziz University, Jeddah, Saudi Arabia
[2] Center of Excellence in Desalination Technology, King Abdulaziz University, P.O. Box 80200, Jeddah 21589, Saudi Arabia
[3] Center for Teaching and Learning Development, King Abdulaziz University, Jeddah, Saudi

Received 02 October 2024
Accepted 05 January 2025
Published 05 February 2025

Corresponding Author
Abdullah H. Kadhum,
hushamabdullah6@gmail.com

DOI
10.29121/ijetmr.v12.i2.2025.1530

Funding: This research received no specific grant from any funding agency in the public, commercial, or not-for-profit sectors.

ABSTRACT

This study examines the energy and performance of a solar sweeping gas membrane distillation (SGMD) unit with different water vapor condensers. The study assesses the efficiency of the SGMD system under different water vapor condensation configurations using only solar energy. The study examines how water vapor condensation configurations affect system productivity, specifically condensed water yield and energy efficiency. The study was conducted in the Mecca area on three occasions: winter, summer, and day. A new model was created to simulate desalination processes, and the research introduced an SGMD unit modeling component to the standard library. The measured and predicted permeate flow values were similar, with peak solar radiation and maximum ambient temperatures. The study yielded good results, with 5,452 W on the latest summer test day and 4,998 W on the latest winter test day. The seawater outflow from the SGMD system was 53-21 degrees Celsius.

Keywords: Sweeping Gas Membrane, Flat Plate Collector, Photovoltaic Panel

1. INTRODUCTION

The lack of water is a vital trouble affecting several parts of the world, especially in regions with dry or semi-dry climates. Elements like rising population numbers, immoderate water consumption, and the ongoing impact of weather change are setting enormous pressure on freshwater supplies Ethaib et al. (2022). Shockingly, three-quarters of the global populace now live in regions where clean ingesting

water is scarce Irki et al. (2020). Renewable power-powered desalination has been identified as a transformative answer for addressing this mission. A regular water supply is vital for selling public fitness, driving financial advancement, ensuring meal safety, lowering poverty, and fostering peace. Adjustments in international weather styles have worsened water scarcity in lots of areas. Consistent with reports from the United Nations, annual water availability has dropped drastically below the important threshold of 1,500 cubic meters in keeping with individual in keeping with year Zubaidi et al. (2022). elevated worldwide demand for water has similarly exacerbated this difficulty Xu et al. (2024). Additionally, the giant use of fossil fuels, mixed with fast urbanization and population boom, has amplified environmental challenges, in particular climate exchange, threatening sustainable development Olabi & Abdelkareem (2022). This case necessitates a shift towards renewable and environmentally friendly power options to sustain societal progress.

Membrane distillation is rising as a progressive and green era, presenting considerable blessings over traditional techniques Lawson & Lloyd (1997). This technique is celebrated for its potential to conserve electricity at the same time as correctly eliminating debris, salts, and microorganisms. not like traditional distillation or reverse osmosis, it operates beneath lower temperature and strain situations. Membrane distillation is characterized by minimal chemical interplay with the answers being processed G. F. W. S. W. H., & Norman N. L. T. M. (n.d.). This thermally pushed procedure separates substances by using a membrane, making it especially suitable for applications in which water is the dominant issue of the solution. In this system, water vapor passes through the tiny pores of a hydrophobic membrane, leaving liquid water at the back. The manner relies on the difference in molecular pressure throughout the membrane's pores, in which one aspect of the membrane at once contacts the feed liquid. A superb feature is that the feed solution cannot penetrate the membrane until the stress exceeds a specific restriction, called the liquid entry stress (LEP) Ren & Wang (2011).

There are 4 number one configurations of membrane distillation systems: direct touch membrane distillation (DCMD), air hole membrane distillation (AGMD), sweeping gas membrane distillation (SGMD), and vacuum membrane distillation (VMD) Basini et al. (1987). The DCMD layout is known for its straightforward setup and minimal equipment desires, making it best for duties like desalinating water or concentrating liquid answers consisting of fruit juices. SGMD and VMD are better desirable for setting apart risky natural compounds or dissolved gases Walton & Solís (n.d.). The AGMD setup, however, gives flexibility and may be utilized in a variety of programs. Membranes utilized in these systems are commonly microporous and water-repellent, made from substances like PTFE, PP, or PVDF. These membranes prevent liquid from coming into their pores due to floor tension, forming a liquid-vapor interface on the pore openings. Versions in the layout of the permeate side—including direct liquid touch, air gaps, or gasoline drift—have an effect on the driving pressure in unique device kinds Essalhi & Khayet (2015).

Membrane distillation membranes may be created by the usage of methods like segment inversion or the mechanical stretching of dense movies. This study makes a specialty of Sweeping Gas Membrane Distillation (SGMD), which makes use of an inert gasoline at the permeate aspect to hold water vapor via the membrane to an outside condenser García-Payo et al. (2002). This approach is green in lowering warmth loss and minimizing resistance to mass switch. Initially, an increase in fuel speed complements the transfer of mass, but in addition, increases can result in a decline. SGMD capabilities by means of channeling vapor to an outside condenser using a gas drift, growing a barrier that limits thermal losses while enhancing vapor

transfer efficiency. This approach is particularly powerful for eliminating risky substances from aqueous solutions Khayet (2011).

But SGMD has its challenges, along with the need for massive condensers due to the small volume of vapor blended with a considerable amount of inert gas. Air, wet air, or dry nitrogen are typically used as sweeping gases, and the gadget's permeability quotes vary from 1 to twenty-five kilograms in step with square meter consistent with hour, depending on the membrane type, the feed solution, and running situations Tomaszewska (2014). elements consisting of feed temperature, flow prices, and membrane properties affect the system's overall performance, with better temperatures significantly boosting vapor strain and, therefore, flow prices. A disadvantage of SGMD is the gradual upward push in fuel temperature in the device, which negatively impacts vapor pressure and decreases the efficiency of the vapor switch. Notwithstanding these challenges, SGMD is powerful for producing distilled or potable water and for putting off risky organic compounds from water-primarily based answers Tomaszewska (2014). Membrane distillation is a system that relies on the distinction in vapor strain throughout a specialized membrane to split freshwater from saline answers, consisting of seawater or underground brine. This approach differs notably from other membrane-based desalination strategies like reverse osmosis, ahead osmosis, electrodialysis, or capacitive deionization, which normally rely on either excessive-stress systems or electrical currents to dispose of salt. Membrane distillation stands out for its top-notch performance in water purification, with blessings along with its flexibility, potential to apply low-first-rate warmness resources, and production of water with very high purity degrees. Its operation at pretty low temperatures helps using renewable electricity, reinforcing its function in sustainable water treatment. One vital aspect affecting the overall performance of membrane distillation structures is the form of condenser used to convert water vapor again into liquid form. Whether the gadget employs a water-cooled warmth exchanger or an exchanger made of polymeric or metallic materials can have an impact on the quality of the final product. Sweeping gasoline membrane distillation (SGMD), a version of this technology, is mainly proper for utilizing warmth from low-temperature resources like solar energy or business waste. In this research, photovoltaic panels and flat-plate solar panels are used to provide each thermal electricity and energy to power the SGMD method. The main aim is to design, evaluate, and optimize an unbiased solar-driven SGMD device ready with exceptional condenser configurations to enhance water production and purity. The study's specific objectives are as follows:

1- The goal is to look at how different types of water-cooled polymetric and metallic exchangers affect the productivity of the system by measuring how much condensed water is produced.

2- To assess the thermal needs for the system's nighttime operation, as well as the energy requirements for photovoltaics (PVs) and solar thermal collectors.

Solar-powered membrane distillation system by Li and Lu Li & Lu (2020) provides fresh water in remote areas without infrastructure. All power comes from the sun. A mathematical model and test results in natural weather conditions were used to evaluate the system. The system produced fresh water at an average rate of 9.98 to 23.26 kilograms per day, with a ratio of flowing air of 4 to 6, a thermal collector efficiency of 50%, three times that of photovoltaic solar panels, and a cost of 18.34 $/m3. They examined heat and moisture transfer in solar-powered water desalination system hollow membrane units using sweeping gas. They also examined how weather and membrane resistance affect moisture transfer driving power and system efficiency. This was done by testing three PVDF membrane units.

The researchers examined membrane parameters like mean pore size, porosity, and tortuosity. They thoroughly examined system performance. They found that fundamental physical characteristics like pore width, porosity, and tortuosity affected system performance. Pore widths were 140–160 micrometers, and porosity was 0.75. In saltwater-accessible areas, Huang et al. Huang et al. (2019) built a treatment plant. Solar membrane distillation energy powered the process. They developed MD using a thermal solar collector and solar panels for thermal and electrical energy. Freshwater cost 85 dollars per cubic meter after SGMD distillation. The system's water unit cost was optimized for 20-year cost recovery. Total cost: $35,000. Many variables were tested, including photovoltaic collector area and flow rates. They found that solar-powered SGMD water production is not cheaper when the thermal or electrical system is stored. They made a smaller hot water tank and a larger thermal accumulator system to increase average operating temperature and lower cost. In membrane evaporation (SGMD), Leelamanie Leelamanie (2011) studied condensation, re-evaporation, and heat transfer. It was shown that membrane characteristics affect condensation and re-evaporation. Membranes with higher mass transfer coefficients—pore size and porosity—condense more. Combined droplet surface area and gas passage speed determine re-evaporation rate. Low gas flow rates increase membrane pore size and evaporation. At higher gas flow rates, the membrane has smaller holes and evaporates faster. Gas flow rate directly affects mass transfer coefficient. As evaporation temperature rises, mass transfer coefficient decreases, but liquid passage speed has little effect. Increasing gas flow or evaporation temperature boosts energy efficiency. SGMD, a novel method that delivers water vapor directly to the root zone, increases soil moisture and agricultural productivity. In practice, sweep gas moves across membrane tube banks' hollow fibers. These tubes carry non-specific fluid in the opposite direction or perpendicular to the membrane surface. The other configuration has sweep gas inside the tubes and hot brine between them. The sweep gas carries thermal saline-produced water vapor to the condenser through the membranes. Condensing water vapor in the condenser produces purified water. Leelaminae Leelamanie (2011) examined how ambient relative humidity affects soil water content, focusing on organic matter and clay content. The study examines how organic matter and clay affect soil moisture availability and retention by correlating soil characteristics and moisture levels. This affects agricultural and environmental management methods that preserve and restore soil moisture and our understanding of soil-water interactions. Boukhriss et al. Boukhriss et al. (2017) studied the SGMD process and found that it can collect hot water for solar distillation despite the capacitor cost. Preliminary research is promising. SGMD has lower conductive heat loss and mass transfer resistance than other MDs. However, Boukhriss et al. Boukhriss et al. (2021) examined how soil moisture levels affected atmospheric water vapor availability and ecosystem evaporation. Ecosystem evaporation transfers water from different ecosystems to the atmosphere as water vapor, mostly by soil evaporation and transpiration. The study examines the atmospheric humidity deficit, the difference between the atmosphere's actual water vapor content and its maximum capacity at a certain temperature. The researchers' theory is that soil moisture deficits reduce evaporation, which raises air humidity deficits. They emphasize that soil moisture and air humidity must be linked to understand how ecosystems control evaporation. Al-Hayeka and Badran examined how relative air wetness affects soil dampness Al-Hayeka & Badran (2004). This study examines how condensation extracts moisture from the sky and affects soil moisture. The main goal is to determine if relative air dampness can be used to increase soil

moisture in dry and semi-arid areas where water is scarce. The study examines how relative air dampness harvest affects soil dampness dynamics and suggests ways to use this method for sustainable water management.

2. METHODOLOGY

The system was simulated using TRNSYS, a software platform specifically designed to model systems with time-dependent behaviors. TRNSYS stands for TRaNsient SYStem and is well-known for its flexibility and versatility. It's widely used for analyzing solar energy systems, building temperature dynamics, electrical grids, HVAC designs, and similar applications. The software treats each system component as an independent "black box" model, making it easier to simulate complex setups. While it was initially created for solar thermal systems, its capabilities have expanded significantly to support a wide variety of dynamic systems Bernier, & Beausoleil-Morrison (2005).

This study examines a gadget comprising a solar flat plate collector, photovoltaic panels, and a sweeping gas membrane distillation (SGMD) unit. The objective is to replace traditional energy sources with renewable alternatives, leading to decentralized desalination methods. Figure 1 illustrates a simplified illustration of the association. The device accommodates two primary components: one committed to power technology and the opposite to desalination. The energy system contains a flat plate collector (FPC), a thermal storage tank prepared with warmth exchangers, pumps, photovoltaic panels with batteries, and a regulator/inverter, all functioning collaboratively to guide the SGMD module. The SGMD unit is significant to the desalination method, with its info addressed in later sections.

In the first phase of the project, we modeled the SGMD unit by creating a custom component for TRNSYS, written as a Fortran subroutine. The second phase involved analyzing how the system performs. Key factors like the temperatures of the input and output streams, as well as the total mass flow rate, were used to measure its efficiency. The system was designed to run full day, making the most of sunlight in Makkah, a city in western Saudi Arabia.

Figure 1

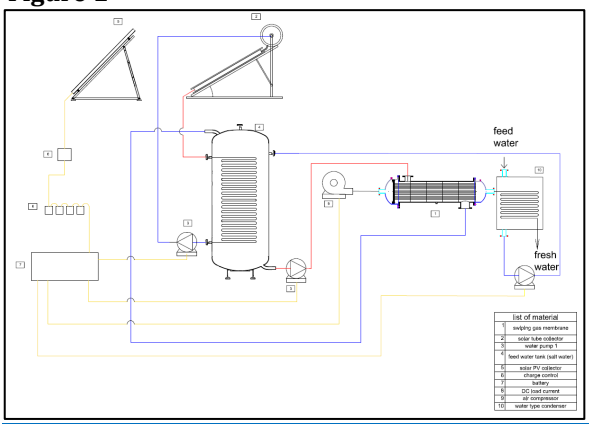

Figure 1 General diagram of the System Setup

2.1. THE SOLAR THERMAL SYSTEM

A flat plate collector (FPC) produces thermal energy, and the heat transfer fluid (HTF) captures solar radiation. The heated fluid functions as a thermal storage

reservoir. The HTF employs a coil heat exchanger for the transfer of heat to saltwater. An FPC functions as a heat exchanger that transforms incoming and diffuse solar radiation into a working fluid, namely a heat transfer fluid (HTF) composed of water and glycol. The Hottel Whillier Bliss equation Vargas-Bautista et al. (2017) delineates thermal efficiency (η_{coil}).

$$\eta_{coil} = a_o - a_1 \frac{(T_3 - T_{amb})}{I_T} - a_2 \frac{(T_3 - T_{amb})^2}{I_T} \quad (1)$$

I_T: the total solar radiation incident (W^1m^{-2}).

a_o: denotes the interception of the efficiency curve, signifying the system's efficiency under optimal circumstances (when there is no temperature differential between the heat transfer fluid and the ambient temperature).

a_1: efficiency slope, first-order coefficient in efficiency equation ($W^{-1}m^2K^1$)

a_2: efficiency curvature, second-order coefficient in efficiency equation ($W^{-1}m^2K^2$).

T_3: temperature at which the fluid enters the collector (°C).

T_{amb}: surrounding temperature (°C).

The most effective method for evaluating the performance of the FPC involves calculating the usable thermal energy (Q_U) transferred from the radiation to the HTF through the FPC, expressed in watts Acevedo et al. (2016).

$$Q_u = m_{HTF} C_{p,HTF} (T_4 - T_3) \quad (2)$$

T_4: outlet temperature of the fluid to the collector (K).

T_3: inlet temperature of the fluid to the collector (K).

m_{HTF}: shows the mass flow rate of the solar fluid ($(KJ\ Kg^{-1}K^{-1})$)

$C_{p,HTF}$: the specific heat capacity of the fluid circulating inside the solar collector ($KJ\ Kg^{-1}K^{-1}$).

η_{coil} may be redefined as:

$$\eta_{coil} = \frac{Qu}{A\ I_T} \quad (3)$$

A: collect surface area of the solar collector (m^2)

The steady-state collector discharge temperature at normal incidence was determined using Equations (1)–(3) as outlined below Acevedo et al. (2016) .

$$T_4 = T_3 + \frac{A}{m_{HFT} C_{p,HFT}} (a_0 I_T + a_1 (T_3 - T_{amb}) - a_2 (T_3 - T_{amb})^2) \quad (3)$$

Following an evaluation of the thermal system's principal component, the flat plate collector (FPC), the focus shifts to the storage tank intended for fluid retention. The system includes an internal heat exchanger designed to capture the advantageous energy from the heat transfer fluid (HTF), along with internal heaters that provide energy as required. The energy balance can be articulated through the subsequent equation Modeling of Solar Storage Tanks. (n.d.) Newton (1995):

$$\boldsymbol{M_i C_{\mathcal{P}} \frac{dT}{dt} = Q_{env} + Q_{Cond} + Q_{hX} + Q_{AUX} + Q_{inject} + Q_{flue}} \quad (4)$$

Q_{env}: the process of energy transfer through convection occurring between the storage tank and the ambient air. (W),

Q_{Cond} : energy transfer occurs by conduction between two layers. (W),

Q_{inject}: the energy transfer associated with the introduction of either warm or cold water into a balloon (W).

Q_{flue}: represents the flow of convective energy exchanged with a potential chimney (W).

Q_{hX}: the amount of energy transfer generated by the heat exchanger (W).

Q_{AUX}: represents the energy output generated by a secondary heater (W)

$C_{\mathcal{P}}$: the fluid within the storage tank's specific heat (kJ Kg^(-1) K^(-1)).

M_i: the mass of water at node i (kg).

Finding a variable-speed pump that adjusts to the quantity of radiation hitting the collection improves the system's performance significantly. The pump's output temperature is calculated as follows Modeling of Solar Storage Tanks. (n.d.):

$$\boldsymbol{T_3 = T_2 + \frac{Q_{HFT}}{m_{HFT}}} \quad (6)$$

T_3: outlet temperature from the pump (°C).

T_2: inlet temperature to the pump (°C).

Q_{HFT}: the energy conveyed from the pump motor to the fluid stream traversing the pump (kJ h^{-1}).

$$\boldsymbol{Q_{HFT} = \mathcal{P}_{shaft}\left(1 - \eta_{pump ing}\right) + \left(\mathcal{P} - \mathcal{P}_{shaft}\right)\mathcal{F}} \quad (5)$$

$\mathcal{P}_{shaft}$: the shaft power required for pumping operations (kJ h^{-1}).

P: the power consumed by the pump at this moment (kJ h^{-1}).

F: represents a portion of the inefficiencies of the pump motor.

$\eta_{pump ing}$: efficiency of fluid pumping.

$$\boldsymbol{P_{afan} = \frac{m_a(\Delta \mathcal{P}_{a,H} + \Delta \mathcal{P}_{a,D})}{\rho_a \eta_{Fan}}} \quad (8)$$

$\Delta P_{a,H}$ and $\Delta P_{a,D}$ symbolize the drops in air pressure above the condenser and the membrane module, respectively Li & Lu (2020).

The sun fraction (SF) is an important performance parameter for the heating system. The definition refers to the ratio of energy given by the solar collector (Q_u) to the total solar energy necessary for the operation of the desalination system, including energy contributed by the auxiliary heater (Q_{AUX}), as indicated in Hobbi, & Siddiqui (2009):

$$SF = \frac{Qu}{Qu+Q_{AUX}} \quad (9)$$

2.2. PHOTOVOLTAIC SOLAR SYSTEM

The electrical system includes solar modules, a battery bank, and an inverter, which converts DC to AC and powers the storage tank's pumps and air compressors. The batteries chemically store direct current electrical energy for later use in cloudy circumstances.

The electric power output (P_PV) from the photovoltaic array, contingent upon irradiance and temperature, is articulated as Ghenai et al. (2018):

$$P_{PV} = P_{PV,STC} F_{STC} \frac{G}{G_{STC}} \left[1 + \alpha_P \left(T_C - T_{C,STC}\right)\right] \quad (6)$$

$P_{PV,STC}$: the output power at the standard test conditions (STC).

F_{STC}: the photovoltaic derating factor.

G: represents the total radiation incident on the photovoltaic array.

G_{STC}: the incident radiation at (STC)

α_P: the temperature coefficient of power.

T_C: the temperature of the photovoltaic module.

$T_{C,STC}$: the temperature of the PV module under standard test conditions (STC)[28]. Standard test conditions (STC): air mass = 1.5, global solar irradiance = 1,000 Wm^{-2}, temperature at STC = 25°C.

Subsequently, the overall PPV of the PV panel is determined. To determine the battery's capacity in ampere-hours (Ah), apply equation (10) as follows Ghenai et al. (2018):

$$Ah = \frac{(P_{LOAD})(N_J)}{(N_b)(P_d)(\mathrm{pr})} \quad (11)$$

P_LOAD is the needed energy during the day (Wh d–1), N_J is the number of autonomous days (1 d with a minimum solar irradiation rate) required, P_(d) is the depth of discharge, N_(b) is the battery efficiency, and pr is the losses.

2.3. SGMD SYSTEM

The hot feed solution enters the SGMD module at a predetermined mass flow rate and temperature. Through the use of air driven by a fan, the gaseous component

of the solution (distillate membrane distillation) passes through the membrane. After that, the vapor travels to the condenser. The hydrophobic microporous fibers were part of the SGMD module. The cylindrical housing encased the fiber tubes. The heated solution moved through the fibers as air moved in a crossflow pattern through the fiber bundle, the porosity is 70% and the pore size is 0.2 μm , as seen in Figure 2 As heat and mass pass through the porous membrane between the two fluids, the temperature of the solution inside the fiber tubes decreases. The concentration increases concurrently along the fiber axis. As a result, the air outside the tube bundle gradually becomes warmer and more humid in the direction that it is moving.

Figure 2

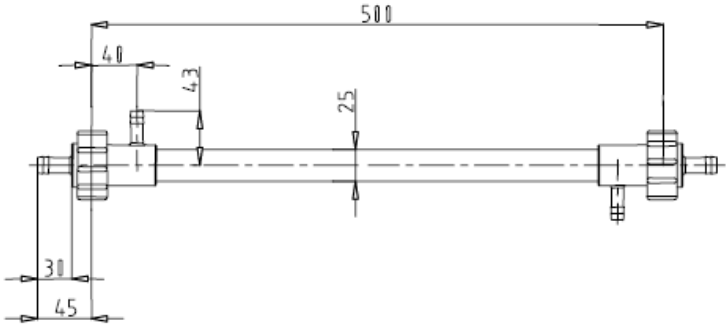

Figure 2 The SGMD Module

An instantaneous fiber-to-fiber model that takes into attention concentration and temperature distributions all through all fiber tubes is challenging to assemble because of the concurrent mass and warmth switch of the technique and the great variety of fiber tubes. A crossflow flat-sheet channel model was used to transform the huge hole fiber tubes right into a flat sheet membrane, hence resolving the issue. While the answer and airstream moved through two parallel channels that had been separated by means of the membrane, as shown in Figure 3, there has been a switch of heat and mass throughout the membrane. There are 3 parts to the SGMD module's general warmth and moisture transfer resistance: the diffusion switch resistance inside the porous membrane, the convective transfer resistances of boundary layers, and the overall bundle Li & Lu (2020).

Figure 3

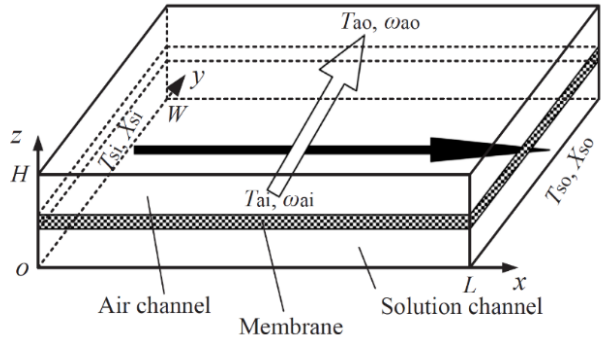

Figure 3 The Computational Scope of the Crossflow flat-Sheet Channel Model [16]

The Reynolds numbers for both the solution and air are far below 2300 during the operation, implying that laminar flow may be used to describe both. References

Li & Lu (2020) and Bergman & Incropera (2011) help one to ascertain 〖Nu〗_f in the solution boundary layer:

$$Nu_f = \frac{h_f d_i}{k_f} = 3.658 + \frac{0.085\left(RePrd_i/L\right)}{1 + 0.047\left(RePrd_i/L\right)^{0.67}} \quad (7)$$

The Nusselt number for air flowing over the fiber bundles can be calculated using a recognized empirical relationship [31]:

$$Nu_p = \frac{h_p d_O}{k_p} = 1.13\, C\, Re_{dO,maX}^{m} Pr_p^{1/3} \quad (8)$$

The constants C and m are associated with the transverse pitch (PT) and longitudinal pitch (PL) of the fiber tubes. For the module with PT/do of 1.5 and PL/do of 1.7, the constants are: C = 0.457, m = 0.564. 〖Re〗_(dO,maX) is defined as the maximum velocity of the airstream inside the fiber bundle Li & Zhang (2017).

The convective moisture transfer coefficient may be derived using the Chilton–Colburn analogy Kays et al. (n.d.).

$$sh = \frac{k_f d_i}{\mathcal{D}} = \frac{Nu_f}{Le^{1/3}} \quad (9)$$

where D is the diffusivity.

The pressure drop of the solution and airstream may be articulated respectively Li & Zhang (2017):

$$\Delta P_{f,\mathcal{H}} = \frac{64}{Re_f}\frac{L}{d_i}\frac{\rho_f u_f^2}{2} \quad (36)$$

$$\Delta P_{p,\mathcal{H}} = f_p N_{\mathcal{L}} \frac{\rho_p u_p^2}{2} \quad (37)$$

u_f is the velocity of the water.

u_p is the velocity of the air.

$\mathcal{N}_{\mathcal{L}}$ is the number of fiber in the air flow movement.

The permeate flow flux can be calculated using the correlation provided below [33].,

$$\mathcal{J} = \mathcal{B}[P_{\mathcal{F}m} - P_{\mathcal{P}m}] \quad (38)$$

where $P_{\mathcal{F}m}$ and $P_{\mathcal{P}m}$ stand for the feed and permeate vapor pressures, respectively, at the corresponding membrane surface temperatures $T_{\mathcal{F}m}$ and $T_{\mathcal{P}m}$.

Consideration has been given to how salt affects vapor pressure. The Knudsen-molecular diffusion model has been used to establish the membrane characteristic parameter B Gryta et al. (1997), Green Social Work, Sieder & Tate (1936), Anderson et al.(2020) because the mean free path of water vapor (~0.13 μm) Zhao et al. (n.d.) is comparable to the mean pore size of the membrane used in the conditions examined in this study.

$$\mathcal{B} = \left[\frac{3\,\tau\delta_m}{2\varepsilon r}\left(\frac{\pi RT}{8M}\right)^{0.5} + \frac{\tau\delta_m}{\varepsilon}\,\frac{Pa}{PD}\,\frac{RT}{M}\right]^{-1}$$

where τ is the tortuosity $\tau = \frac{(2-\varepsilon)^2}{\varepsilon}$ Kim et al. (2021), δ_m is the thickness of membrane (m) , ε is the porosity , R is the universal gas constant (J $mole^{-1}K^{-1}$), T is the bulk temperature in (K) , Pa air pressure (pa), P total pressure (pa) , D is the diffusivity (m^2s^{-1}) Nasirabadi et al. (2016), M is molecular weight (kg $mole^{-1}$).

Membrane surface temperatures may be computed using the following relationships, based on feed and permeate temperatures and different heat transfer coefficients Saturation thermodynamic properties of water at. (n.d.) Qtaishat et al. (2008).

$$T_{\mathcal{F}m} = T_{\mathcal{F}} - (T_{\mathcal{F}} - T_{\mathcal{P}})\frac{1/h_{\mathcal{F}}}{\frac{1}{h_V + h_C} + \frac{1}{h_{\mathcal{P}}} + \frac{1}{h_{\mathcal{F}}}} \qquad (10)$$

$$T_{\mathcal{P}m} = T_{\mathcal{P}} - (T_{\mathcal{F}} - T_{\mathcal{P}})\frac{1/h_{\mathcal{P}}}{\frac{1}{h_V + h_C} + \frac{1}{h_{\mathcal{P}}} + \frac{1}{h_{\mathcal{F}}}} \qquad (11)$$

In this context, $h_{\mathcal{F}}$ and $h_{\mathcal{P}}$ denote the heat transfer coefficients on the feed and permeate sides, respectively, whereas h_V and h_C refer to the vapor and membrane heat transfer coefficients. h_V can be determined using the following correlation.

$$h_V = \frac{J\Delta\mathcal{H}V}{T_{\mathcal{F}m} - T_{\mathcal{P}m}} \qquad (42)$$

The vapor enthalpy ΔHV at the average membrane temperature can be calculated using the following correlation.

$$\Delta\mathcal{H}V = (1.7535\left(\frac{T_{\mathcal{F}m} + T_{\mathcal{P}m}}{2}\right) + 2024.3 \qquad (12)$$

$$h_C = \frac{k_m}{\delta_m} \qquad (44)$$

where the k_m is thermal conductivity of the membrane Ali et al. (2015). Equations (Anderson et al. (2020),Kim et al. (2021) and Nasirabadi et al. (2016)) have been resolved via the iterative technique as proposed in Martínez-Díez & Vázquez-González (1999).

Using the feed and permeate streams' heat and mass balances, we were able to determine temperature profiles along the fiber. The energy difference between the feed side's input and output is transferred across the membrane by conduction and convection Saturation thermodynamic properties of water at. (n.d.) Qtaishat et al. (2008).

$$m_f Cp_f T_i - m_f Cp_f T_{i+1} = h_c(T_{fm} - T_{pm})dA + J\Delta H_v dA \quad (13)$$

$$T_{fi+1} = \frac{m_f Cp_f T_{fi} - (h_c(T_{fm} - T_{pm})dA + J\Delta H_v dA)}{m_f Cp_f} \quad (14)$$

In a similar manner, the temperature of the permeate

$$T_{pi+1} = \frac{m_p Cp_p T_{pi} - (h_c(T_{fm} - T_{pm})dA + J\Delta H_v dA)}{m_p Cp_p} \quad (15)$$

To determine the ((P_{fm} and P_{pm}), it is necessary to adhere to the guidelines outlined in references Saturation thermodynamic properties of water at. (n.d.) and Qtaishat et al. (2008).

$$P_{fm} = \exp\left(23.1964 - \frac{3816.44}{T_{fm} - 46.13}\right) \quad (16)$$

$$P_{pm} = \exp\left(23.1964 - \frac{3816.44}{T_{pm} - 46.13}\right) \quad (17)$$

2.4. THE MODELING OF THE SOLAR SGMD SYSTEM USING TRNSYS

A hybrid solar thermal and photovoltaic SGMD system, as illustrated in Figure 4, was designed and tested using TRNSYS version 18. An FPC (Type 73) is part of the solar thermal system,

Figure 4

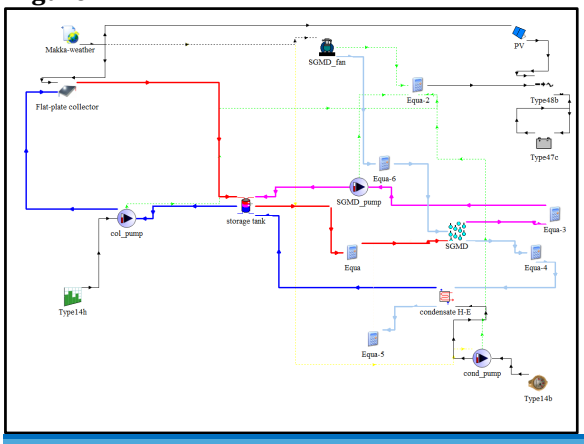

Figure 4 TRNSYS Diagram

Fourteen forcing functions, water resources (Type 14b), Type 14h immersion heater control signals, a Type 60r stratified fluid storage tank including two inlets and one outlet, a Type 110 variable-speed water pump, along with optional internal heaters and heat exchangers. The TRNSYS standard component encompasses the electrical power systems utilized in this work, comprising solar panels (TYPE103), electrical storage (TYPE47c), and regulator/inverter (TYPE48b). Supplementary components comprise a unit conversion mechanism, Type 65c online plotters with files, TYPE15-TMY2 weather data acquisition and processing, and the TYPE24 integrator. This research has led to the inclusion of TYPE 1996 in the standard library, a newly designed component for representing an SGMD unit. This indicates that our research made a substantial contribution. This component was developed using the FORTRAN programming language. The subsequent section includes tables detailing PV panels (EURONET) with a maximum rated power of 115 W and a maximum power point voltage of 17.4 V.

3. RESULTS AND DISCUSSION

This study includes validating and simulating the plant for a year in Makkah, Saudi Arabia. To simplify the presentation of the results, three dates were chosen: January 20th, May 15th, and June 15th. Figure 5 shows the Ambient temperatures (degrees Celsius) are considered as one of the basic pillars that should be measured and were measured during the three tested days (20 January), (15 May) and (15 June) and the highest temperatures recorded during the three days were 32.4°C, 39.2°C, 39.5 °C, respectively.

Figure 5

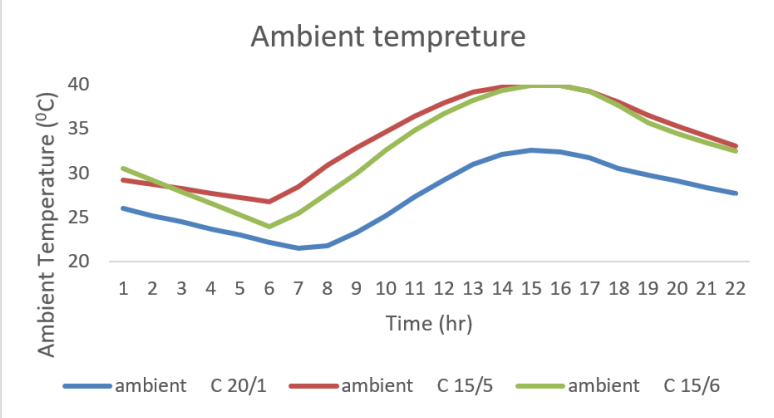

Figure 5 Ambient temperature

The thermal energy captured by the flat plate collector is used to heat the water exiting the solar collector. Figure 6 depicts a simulation of a model that uses the available solar energy from solar thermal collectors to heat the HTF over the months of January, May, and June. We observe a drop in temperature in January.

Figure 6

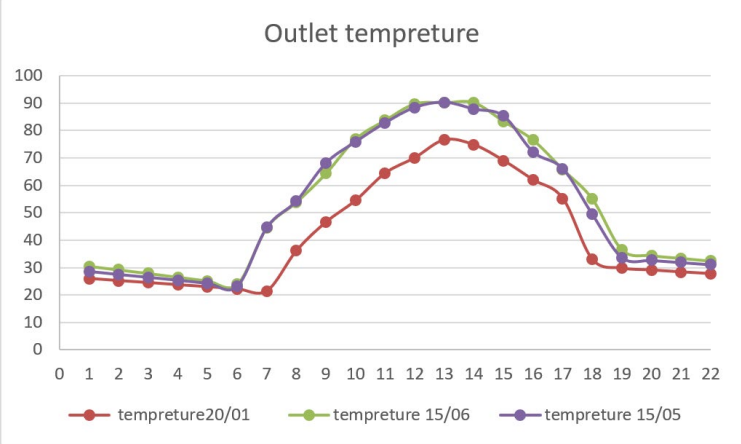

Figure 6 Outlet Temperature from Collector

Figure 7 depicts the amount of condensed water and the temperature of the water entering the SGMD using glass condenser, demonstrating a direct relationship between increasing temperature and the amount of water condensation. These values were compared to the practical findings obtained in the laboratory to ensure the TRNSYS program's accuracy.

Figure 7

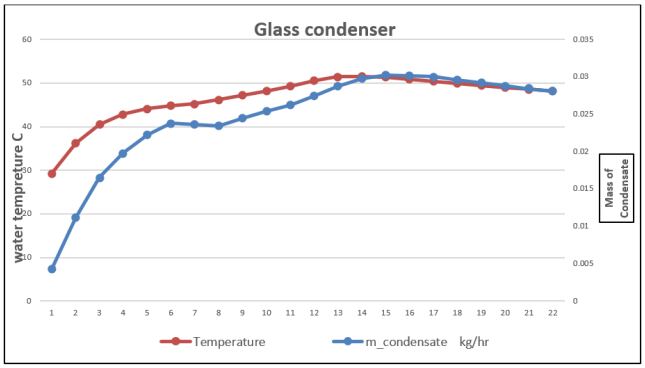

Figure 7 The amount and Temperature of Condensed water Entering SGMD via Glass Condenser

Figure 8,Figure 10 illustrate the inlet water temperature and mass condensate to the membrane utilizing the copper water condenser for the months of January, May, and June. The temperature curves of the inlet water exhibit slight variations when utilizing the copper water condenser in the membrane during January, May, and June. The initial mass was low because of the low water temperature, and as the water temperature rose, the quantity of condensed water increased. The quantity of condensed water exhibits a slight reduction in the afternoon, coinciding with a decrease in temperature after 3 pm.

Figure 8

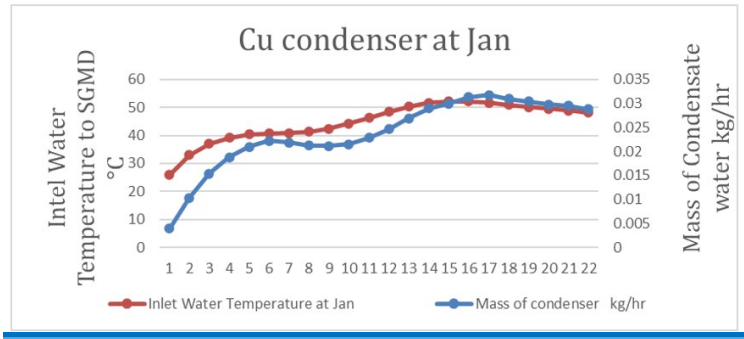

Figure 8 Inlet Water Temperature and Mass Condensate to the Membrane Using the Copper Water Condenser in January

Figure 9

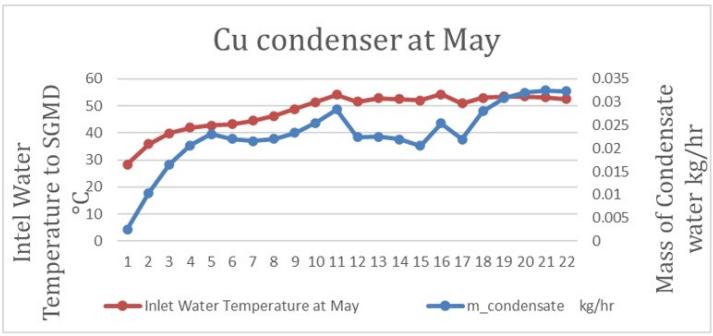

Figure 9 Inlet Water Temperature and Mass Condensate to the Membrane Using the Copper Water Condenser in May

Figure 10

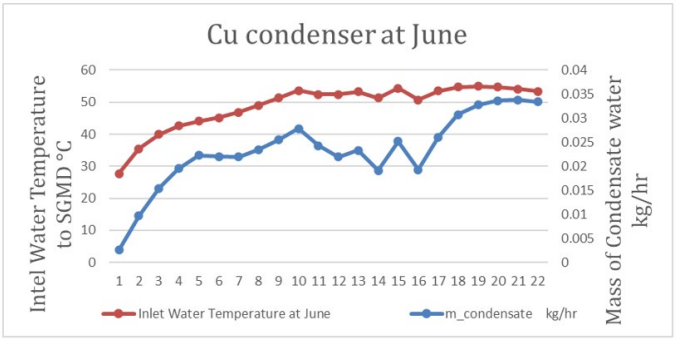

Figure 10 Inlet Water Temperature and Mass Condensate to the Membrane Using the Copper Water Condenser in June

Figure 11-Figure 13 illustrate the amount of water condensed in polypropylene across three different months, coupled with the inlet water temperature to SGMD on the specified dates of January 20, May 15, and June 15. The peak of condensation occurred in June, during the hottest hours of the day. The relationship is direct, indicating that the condensed mass increases with rising temperature. We notice that utilizing a copper condenser produces more condensed water than using a polymer condenser. This is due to copper's high heat conductivity, which causes more heat exchange, resulting in more condensed water.

Figure 11

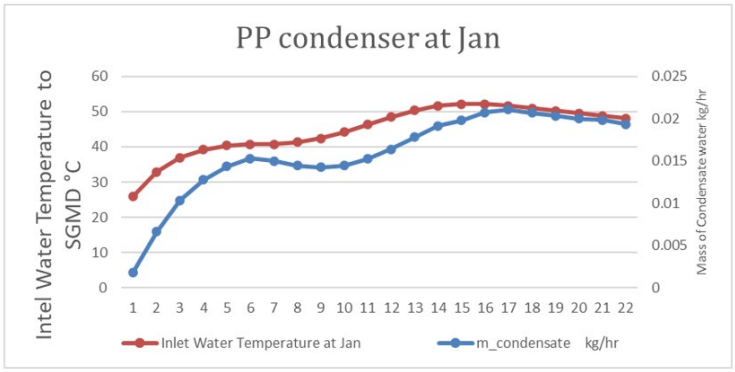

Figure 11 Inlet Water Temperature and Mass Condensate to the Membrane Using the PP Condenser in January

Figure 12

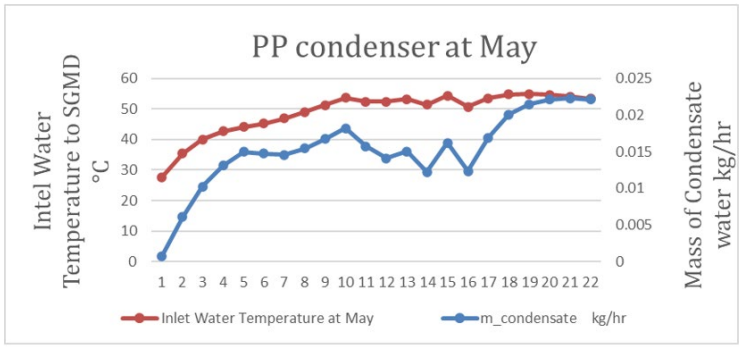

Figure 12 Inlet Water Temperature and Mass Condensate to the Membrane Using the PP Condenser in May

Figure 13

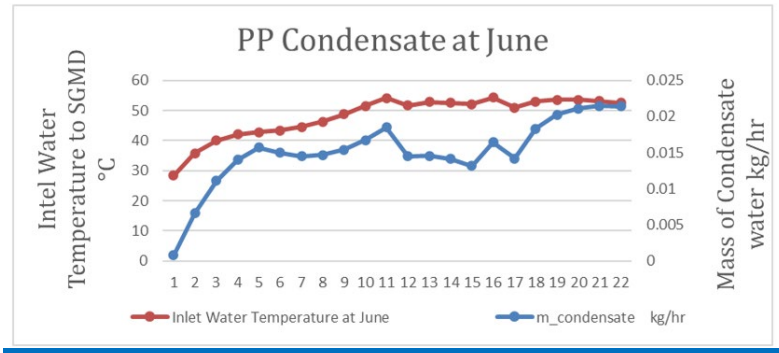

Figure 13 Inlet Water Temperature and Mass Condensate to the Membrane Using the Pp Condenser in June

Figure 14 illustrates the useful power gain from FPC on the designated dates of January 20, May 15, and June 15. The findings indicate that the maximum reached 555 W at 1:00 PM during the summer. It progressively diminished alongside the reduction in solar radiation, as evidenced throughout all testing days.

Figure 14

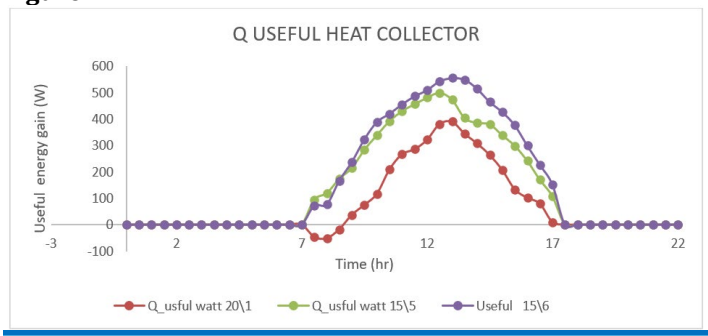

Figure 14 Q the useful Power Gain from FPC on January 20, May 15, and June 15

The solar energy falling on the solar collector heats the water, which then heats the water in the tank. This falling energy varies by month of the year, with the highest value in June and the lowest in January. Figure 15 illustrates the solar radiation on a surface tilted at 30 degrees. The data indicates that the peak radiation occurred at 13:00 in June, reaching 994.9 W/m2. In May, the highest recorded value was 897 W/m2 at 12:00 noon, while in January, the maximum was 786.6 W/m2, also at 12:00 noon.

Figure 15

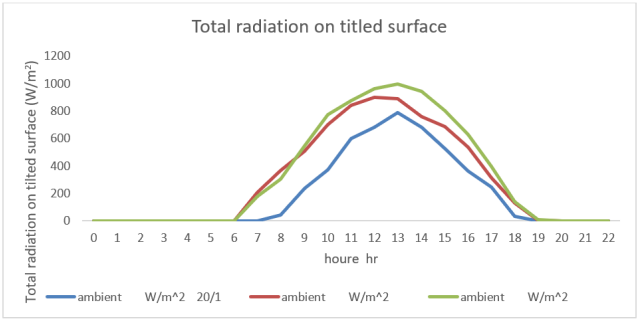

Figure 15 Total Radiation on the Surface tilted at 30 Degrees

Figure 16 illustrates that the temperature of the water exiting the tank to the SGMD increases progressively from 20 °C to 54 °C throughout the day, as depicted in the figure for the tested months of the year. The temperature remained elevated at night due to the presence of an electrical heater in the thermal storage tank, which sustains the temperature.

Figure 16

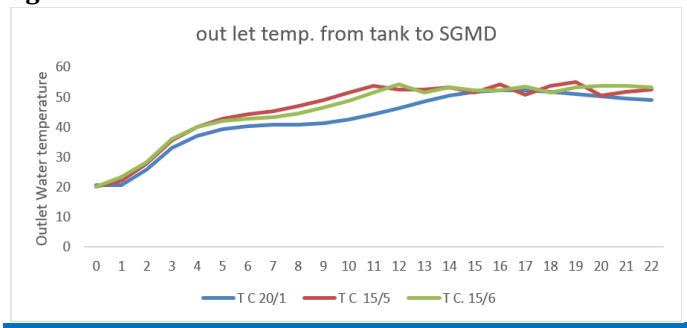

Figure 16 Temperature of the Water Exiting the Tank to the SGMD

A comprehensive understanding of the solar array's daily operation will enhance the ability to identify optimal times for utilizing solar energy to maximize efficiency. To assess the efficiency of the thermal collector, the equation η = Qu/AI is employed. Figure 17 illustrates a detailed analysis of the thermal collector's efficiency. In June, the highest values were recorded, while January, recognized as the month with the lowest temperatures relative to other months, recorded the lowest values.

Figure 17

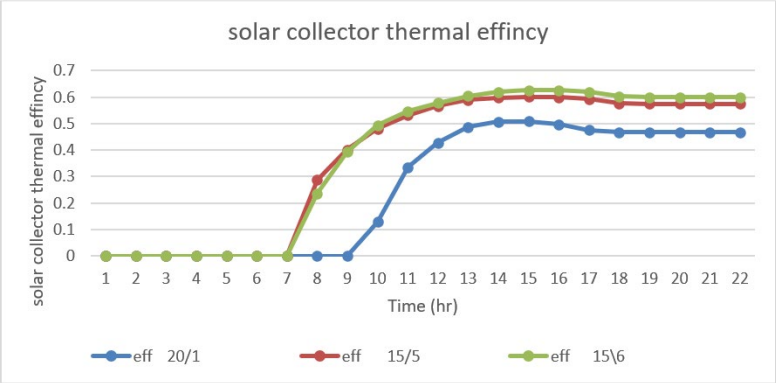

Figure 17 Thermal Efficiency of Solar Collector

The electrical energy produced by the solar panels powered the entire system of pumps and auxiliary heaters. Figure 18-Figure 20 illustrate the power generated from photovoltaic systems during daytime hours in January, May, and June. The power progressively escalates, attaining peak values of 4998, 5452, and 5452 W, respectively. This energy will power the necessary components of the system during daylight, including the thermal heaters, while the surplus will be stored in batteries for nighttime use to operate the thermal heaters. The heaters are utilized during the day as necessary and at night to heat the water.

Figure 18

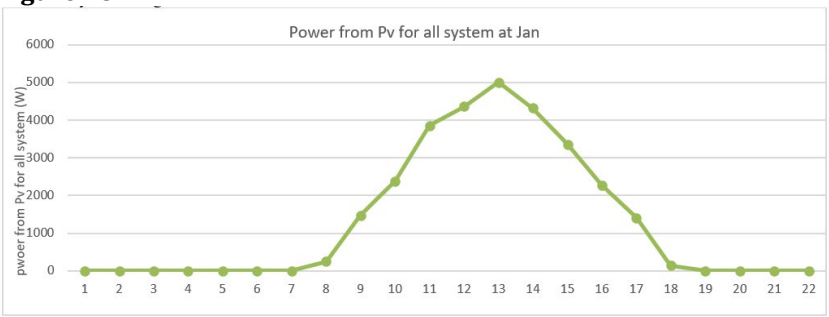

Figure 18 Power Generated from Photovoltaic Systems During Daytime Hours in January

Figure 19

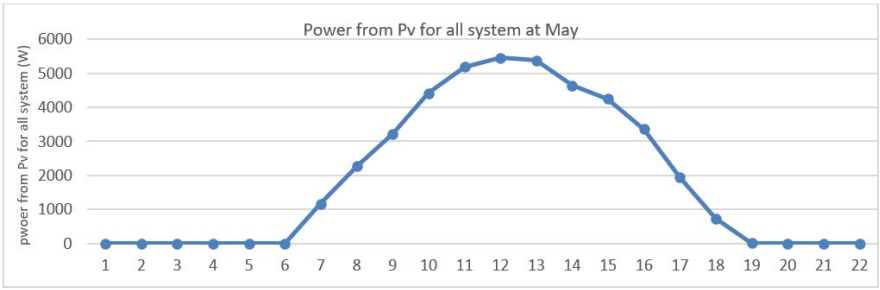

Figure 19 Power Generated from Photovoltaic Systems During Daytime Hours in May

Figure 20

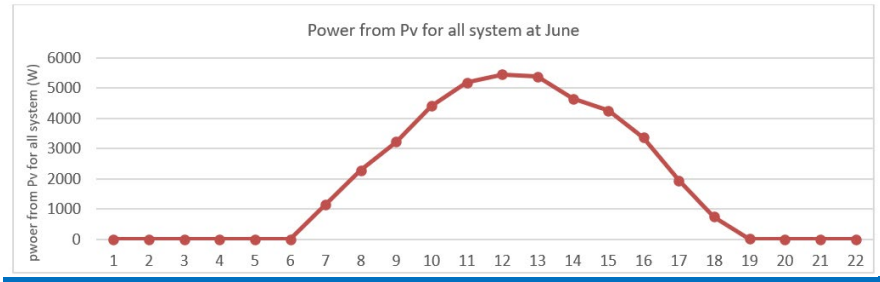

Figure 20 Power Generated from Photovoltaic Systems During Daytime Hours in June

4. MODEL VALIDATION OF SGMD MODULE AND THERMAL SYSTEM

The SGMD model was validated through many simulations with different membrane lengths and pore sizes of 0.2 μm. We compared the projected results from our modeling to the experimental research results of Mohamed Emad, a master's student at King Abdulaziz University's Center of Excellence in Desalination Technology Eltahlawi (n.d.). This comparison demonstrates that the differences between Mohamed's experimental results and our numerical results from the SGMD model were minimal when both our model and his experiments incorporated the following features. In Mohamed Emad's study, a water flow rate of 2.4 liters per minute at a temperature of 51.4 degrees Celsius and air at a flow rate of 10 liters per minute at a temperature of 27 degrees Celsius were used. Mohamed relied on electrical energy as the power source to operate the system and employed a glass helical in shell heat exchanger condenser to obtain the condensed water. In our model, the feed flow rate was 2.4 liters per minute, the air flow rate was 10 liters per minute, with cold inlet temperatures at 27 °C and hot inlet temperatures at 51.4 °C. The fluid flow rate was measured at 2.4 liters per minute, and the total membrane length was 0.5 meters and used a glass helical in shell heat exchanger condenser to obtain the condensed water. The results demonstrated a strong alignment between our numerical model and the experimental results, achieving consistency, resulting in similar outcomes for the collected water condensate, with an uncertainty rate of 98%.

5. CONCLUSION

This study investigated solar thermal and photovoltaic systems integrated with an SGMD unit. A system was developed and evaluated using TRNSYS version 18 to

generate freshwater from brackish water with solar collector (FPC), photovoltaic (PV), and SGMD technologies. Throughout the year, adjustments to the research case for the Makkah area in Saudi Arabia were made on three specific days: winter (January 20th), summer (May 15th and June 15th). Due to the insufficient capacity of TRNSYS in modeling desalination processes, a new model was developed to conduct comprehensive simulations. This study resulted in the addition of a newly developed component for modeling an SGMD unit to the standard library. This indicates that our research has had a substantial impact. The observed and expected permeate flow measurements are notably similar. The maximum total solar radiation recorded on these days was 994.9, 897, and 786.6 W m-2, with corresponding maximum ambient temperatures of 32.4 °C, 39.5 °C, and 39.2 °C, respectively. On this winter's day (January 20th), the temperature at the collector's output fluctuates between 20 and 78 degrees Celsius. On a summer day (June 15th), the collector's outflow temperature peaks at 90 °C and descends to a minimum of 20°C, with a range spanning from 20 °C to 90 °C. Over the three-day operation, the FPC field attains maximum useful energy gains of 400 W, 555 W, and 500 W, with corresponding collector efficiencies of 62%, 60%, and 50%. A full day of auxiliary heating utilized the same maximum value of 12,000 kJ h-1. The anticipated maximum power point (MPP) for a photovoltaic (PV) system may attain 3,680 watts. Results were satisfactory, reaching 5,452 W on the most recent summer test day and 4,998 W on the most recent winter test day. The seawater outflow temperature of the SGMD system varies from 53 to 21 degrees Celsius. The daily distillate yield is 0.0338 kg/hr with a Cu condenser and 0.021 kg/hr with a PP condenser for this experiment. The results are a portion of an extensive study on solar desalination.

CONFLICT OF INTERESTS

None.

ACKNOWLEDGMENTS

None.

REFERENCES

Acevedo, L., et al. (2016). Dynamic Simulation of a Trigeneration Scheme for Domestic Purposes Based on Hybrid Techniques. Energies, 9(12), 1013. https://doi.org/10.3390/EN9121013

Al-Hayeka, I., & Badran, O. O. (2004). The Effect of Using Different Designs of Solar Stills on Water Distillation. Desalination, 169(2), 121-127. https://doi.org/10.1016/J.DESAL.2004.08.013

Ali, A., Aimar, P., & Drioli, E. (2015). Effect of Module Design and Flow Patterns on Performance of Membrane Distillation Process. Chemical Engineering Journal, 277, 368-377. https://doi.org/10.1016/j.cej.2015.04.108

Anderson, D. A., Tannehill, J. C., Pletcher, R. H., Ramakanth, M., & Shankar, V. (2020). Computational Fluid Mechanics and Heat Transfer. https://doi.org/10.1201/9781351124027

Basini, L., D'Angelo, G., Gobbi, M., Sarti, G. C., & Gostoli, C. (1987). A Desalination Process Through Sweeping Gas Membrane Distillation. Desalination, 64, 245-257. Accessed: Sep. 09, 2024. [Online]. Available:

Bergman, T. L., & Incropera, F. P. (2011).Fundamentals of Heat and Mass Transfer* (1048). Accessed: Oct. 26, 2024. [Online]. Available:

Bernier, M., & Beausoleil-Morrison, I. (2005). New Evolutions in TRNSYS: A Selection of Version 16 features.

Boukhriss, M., Zarzoum, K., Maatoug, M. A., & Timoumi, M. (2021). Innovation of Solar Desalination System Coupled with Solar Collector: Experimental Study. Journal of Advanced Research in Fluid Mechanics and Thermal Sciences, 80(1), 94-111. Accessed: Sep. 10, 2024. [Online]. Available:

Boukhriss, M., Zhani, K., & Ben Bacha, H. (2017). Optimization of Membrane Distillation (MD) Technology for Specific Application Desalination. International Journal of Advanced Manufacturing Technology, 88(1-4), 55-66. https://doi.org/10.1007/S00170-016-8756-4/METRICS

Eltahlawi, M. E. (n.d.). Experimental Investigations on Topsoil Humidification by a Sweeping Gas Membrane Distillation System (Unpublished thesis). King Abdulaziz University, Jeddah.

Essalhi, M., & Khayet, M. (2015). Membrane Distillation (MD). In Progress in Filtration and Separation (pp. 61-99). https://doi.org/10.1016/B978-0-12-384746-1.00003-3

Ethaib, S., Zubaidi, S. L., & Al-Ansari, N. (2022). Evaluation Water Scarcity Based on GIS Estimation and Climate-Change Effects: A Case Study of Thi-Qar Governorate, Iraq. Cogent Engineering, 9(1). https://doi.org/10.1080/23311916.2022.2075301

G. F. W. S. W. H., & Norman N. L. T. M. (n.d.). Advanced Membrane Technology and Applications.

García-Payo, M. C., Rivier, C. A., Marison, I. W., & Von Stockar, U. (2002). Separation of Binary Mixtures by Thermostatic Sweeping Gas Membrane Distillation: II. Experimental Results with Aqueous Formic Acid Solutions. Journal of Membrane Science, 198(2), 197-210. https://doi.org/10.1016/S0376-7388(01)00649-4

Ghenai, C., Merabet, A., Salameh, T., & Pigem, E. C. (2018). Grid-tied and stand-alone hybrid solar power system for desalination plant. Desalination, 435, 172-180. https://doi.org/10.1016/J.DESAL.2017.10.044

Gryta, M., & Tomaszewska, M. (1998). Heat Transport in the Membrane Distillation Process. Journal of Membrane Science, 144 (1-2), 211-222. https://doi.org/10.1016/S0376-7388(98)00050-7

Gryta, M., Tomaszewska, M., & Morawski, A. W. (1997). Membrane Distillation with Laminar Flow. Separation and Purification Technology, 11(2), 93-101. https://doi.org/10.1016/S1383-5866(97)00002-6

Hobbi, A., & Siddiqui, K. (2009). Optimal Design of a Forced Circulation Solar Water Heating System for a Residential Unit in Cold Climate Using TRNSYS. Solar Energy, 83(5), 700-714. https://doi.org/10.1016/J.SOLENER.2008.10.018

Huang, S. M., et al. (2019). Heat and Mass Transfer in a Hollow Fiber Membrane Contactor for Sweeping Gas Membrane Distillation. Separation and Purification Technology, 220, 334-344. https://doi.org/10.1016/J.SEPPUR.2019.03.046

Irki, S., Kasbadji-Merzouk, N., Hanini, S., & Ghernaout, D. (2020). Modelling of the Coupling of Desalination Plants with the Thermal Solar Energy System. Water Science and Technology: Water Supply, 20(5), 1807-1822. https://doi.org/10.2166/ws.2020.092

Kays, W. M., Crawford, M. E., & Weigand, B. (n.d.). Solutions Manual.

Khayet, M. (2011). Membranes and Theoretical Modeling of Membrane Distillation: A Review. Advances in Colloid and Interface Science, 164(1-2), 56-88. https://doi.org/10.1016/J.CIS.2010.09.005

Kim, W. J., Campanella, O., & Heldman, D. R. (2021). Predicting the Performance of Direct Contact Membrane Distillation (DCMD): Mathematical Determination of Appropriate Tortuosity Based on Porosity. Journal of Food Engineering, 294, 110400. https://doi.org/10.1016/J.JFOODENG.2020.110400

Lawson, K. W., & Lloyd, D. R. (1997). Review Membrane distillation.

Leelamanie, D. (2011). Changes in Soil Water Content with Ambient Relative Humidity in Relation to the Organic Matter and Clay. Tropical Agricultural Research and Extension, 13(1), 6. https://doi.org/10.4038/TARE.V13I1.3130

Li, G. P., & Zhang, L. Z. (2017). Conjugate Heat and Mass Transfer in a Cross-Flow Hollow Fiber Membrane Bundle used for Seawater Desalination Considering Air Side Turbulence. Journal of Membrane Science, 533, 321-335. https://doi.org/10.1016/J.MEMSCI.2017.03.051

Li, G., & Lu, L. (2020). Modeling and Performance Analysis of a Fully Solar-Powered Stand-Alone Sweeping Gas Membrane Distillation Desalination System for Island and Coastal Households. Energy Conversion and Management, 205. https://doi.org/10.1016/j.enconman.2019.112375

MICRODYN Microfiltration Modules. (n.d.). Accessed: Oct. 26, 2024.

Martínez-Díez, L., & Vázquez-González, M. I. (1999). Temperature and Concentration Polarization in Membrane Distillation of Aqueous Salt Solutions. Journal of Membrane Science, 156*(2), 265-273. https://doi.org/10.1016/S0376-7388(98)00349-4

Modeling of Solar Storage Tanks. (n.d.). Accessed: Oct. 24, 2024. [Online]. Available:

Nasirabadi, P. S., Jabbari, M., & Hattel, J. H. (2016). Estimation of Water Diffusion Coefficient into Polycarbonate at Different Temperatures Using Numerical Simulation. In AIP Conference Proceedings*. https://doi.org/10.1063/1.4951801

Newton, B. J. (1995). Modeling of Solar Storage Tanks. Accessed: Oct. 24, 2024. [Online]. Available:

Olabi, A. G., & Abdelkareem, M. A. (2022). Renewable Energy and Climate Change. Renewable and Sustainable Energy Reviews, 158, 112111. https://doi.org/10.1016/J.RSER.2022.112111

Qtaishat, M., Matsuura, T., Kruczek, B., & Khayet, M. (2008). Heat and Mass Transfer Analysis in Direct Contact Membrane Distillation. Desalination, 219*(1-3), 272-292. https://doi.org/10.1016/J.DESAL.2007.05.019

Ren, J., & Wang, R. (2011). Preparation of Polymeric Membranes. In Membrane and Desalination Technologies (pp. 47-100). https://doi.org/10.1007/978-1-59745-278-6_2

Saturation thermodynamic properties of water at. (n.d.).

Sieder, E. N., & Tate, G. E. (1936). Heat Transfer and Pressure Drop of Liquids in Tubes. Industrial & Engineering Chemistry, 28(12), 1429-1435. https://doi.org/10.1021/IE50324A027/ASSET/IE50324A027.FP.PNG_V03

Tomaszewska, M. (2014). Sweep Gas Membrane Distillation (SGMD). In Encyclopedia of Membranes (1-3). https://doi.org/10.1007/978-3-642-40872-4_769-2

Tomaszewska, M. (2014). Sweep Gas Membrane Distillation (SGMD). In Encyclopedia of Membranes (1-3). https://doi.org/10.1007/978-3-642-40872-4_769-2

Vargas-Bautista, J. P., García-Cuéllar, A. J., Pérez-García, S. L., & Rivera-Solorio, C. I. (2017). Transient Simulation of a Solar Heating System for a Small-Scale Ethanol-Water Distillation Plant: Thermal, Environmental and Economic

Performance. Energy Conversion and Management, 134, 347-360. https://doi.org/10.1016/J.ENCONMAN.2016.12.041

Walton, J. C., & Solís, S. S. (n.d.). Solar and Waste Heat Desalination by Membrane Distillation. [Online]. Available: https://www.researchgate.net/publication/267196192

Xu, G., Yang, M., Li, S., Jiang, M., & Rehman, H. (2024). Evaluating the Effect of Renewable Energy Investment on Renewable Energy Development in China with Panel Threshold Model. Energy Policy, 187, 114029. https://doi.org/10.1016/J.ENPOL.2024.114029

Yun, Y., Ma, R., Zhang, W., Fane, A. G., & Li, J. (2006). Direct Contact Membrane Distillation Mechanism for High Concentration NaCl Solutions. Desalination, 188(1-3), 251-262. https://doi.org/10.1016/J.DESAL.2005.04.123

Zhao, S., Feron, P. H. M., Xie, Z., Zhang, J., & Hoang, M. (n.d.). Condensation Studies in Membrane Evaporation and Sweeping Gas Membrane Distillation.

Zubaidi, S. L., Hashim, K., Ethaib, S., Al-Bdairi, N. S. S., Al-Bugharbee, H., & Gharghan, S. K. (2022). A Novel Methodology to Predict Monthly Municipal Water Demand Based on Weather Variables Scenario. Journal of King Saud University - Engineering Sciences, 34(3), 163-169. https://doi.org/10.1016/J.JKSUES.2020.09.011